4-15-2016

Removal of Arsenic from water using synthetic Fe7S8 nanoparticles

Jesus Cantu
The University of Texas Rio Grande Valley

Louis E. Gonzalez
The University of Texas Rio Grande Valley

Jacqueline Goodship
The University of Texas Rio Grande Valley

Monica Contreras
The University of Texas Rio Grande Valley

Meera Joseph
The University of Texas Rio Grande Valley

See next page for additional authors

Recommended Citation

Cantu, Jesus et al. "Removal of Arsenic from water using synthetic Fe7S8 nanoparticles." Chemical engineering journal (Lausanne, Switzerland : 1996) vol. 290 (2016): 428-437. doi:10.1016/j.cej.2016.01.053

HHS Public Access

Author manuscript

Chem Eng J. Author manuscript; available in PMC 2017 April 15.

Published in final edited form as:

Chem Eng J. 2016 April 15; 290: 428–437. doi:10.1016/j.cej.2016.01.053.

Removal of Arsenic from water using synthetic Fe_7S_8 nanoparticles

Jesus Cantu, **Louis E. Gonzalez**, **Jacqueline Goodship**, **Monica Contreras**, **Meera Joseph**, **Cameron Garza**, **T.M. Eubanks**, and **J.G. Parsons***

Department of Chemistry University of Texas Rio Grande Valley 1201 West University, Dr. Edinburgh TX 78539

Abstract

In the present study, pyrrhotite was used to remove arsenite and arsenate from aqueous solutions. The Fe_7S_8 was synthesized using a solvothermal synthetic method and it was characterized using XRD and SEM micrographs. Furthermore, the particle size for the nanomaterial Fe_7S_8 was determined to be 29.86 ± 0.87 nm using Scherer's equation. During the pH profile studies, the optimum pH for the binding of As (III) and As (V) was determined to be pH 4. Batch isotherm studies were performed to determine the binding capacity of As(III) and As(V), which was determined to be 14.3 mg/g and 31.3 mg/g respectively for 25°C. The thermodynamic studies indicated that the ΔG for the sorption of As(III) and As(V) ranged from −115.5 to −0.96 kJ/mol, indicating a spontaneous process was occurring. The enthalpy indicated that an exothermic reaction was occurring during the adsorption in which the ΔH was −53.69 kJ/mol and −32.51 kJ/mol for As(III) and As(V) respectively. In addition, ΔS values for the reaction had negative values of −160.46 J/K and −99.77 J/K for the adsorption of As(III) and As(V) respectively which indicated that the reaction was spontaneous at low temperatures. Furthermore, the sorption for As(III) and As(V) was determined to follow the second order kinetics adsorption model.

Keywords

Arsenic sorption; Fe_7S_8; thermodynamics; kinetics; isotherms

1 Introduction

Inorganic and organic forms of arsenic exist ubiquitously in nature. There are two commonly encountered oxidation states of arsenic: As (III) and As (V), wherein As (III) is 25–60 times more toxic than As (V) [1]. Elevated concentrations of arsenic in the environment have been attributed to arsenical herbicides, the combustion of fossil fuels, and the release of arsenic during mining and smelting operations [2, 3]. Arsenic released though different anthropogenic and natural processes can potentially contaminate groundwater, surface water,

Corresponding Author: Phone (956)-665-7462 jason.parsons@utrgv.edu.

terrestrial, and marine environments, which can have lethal effects on organisms. In addition, arsenic has also been linked to the development of various forms of cancer such as skin, bladder, liver, and lung [4]. Aside from being carcinogenic, arsenic has also been linked to non-cancerous multi-systemic health issues such as dermal diseases, cardiovascular disease, hypertension, and diabetes mellitus [4, 5]. This phenomenon has made arsenic a major concern in both environmental and human health. As a result of the potential human and environment health issues associated with arsenic the search for more efficient methods to remove arsenic contaminants from potable water has become a major research focus. In addition, the U.S. Environmental Protection Agency (EPA) reduced the maximum arsenic contaminant level from 50 ppb to 10 ppb in response to the serious known adverse health effects in 2001 [3].

Currently, there are various technologies used to remove arsenic from the environment which include: adsorption, anion exchange, and precipitation. Current anion-exchange resins are generally non-specific and very expensive. As well there are issues with the use of precipitating agents for water treatment, such as adding a chemical to water during the treatment which has to be removed. In addition, the use of precipitating agents in water treatment also generates toxic sludge, which had to be treated and disposed of in the correct manner. However, adsorption technology has shown much promise for the remediation of contaminates from water. Adsorption technologies based on metal oxides and metal sulfides have shown much promise in the remediation of heavy metals from water.

Many different materials have been studied for their potential to remove ions from water for example; aluminum oxide/oxyhydroxides, water treatment residuals, zero valent iron nanoparticles, iron oxides, granulated ferric oxide (GFO), iron oxyhydroxides, manganese oxides, activated carbon, red mud, activated carbon, transition metal sulfides, and many other supported and unsupported materials have been investigated [3, 6–26]. These different materials have been shown to have high binding affinities for metals ions including As(III)/As(V) [3,6–26]. However, Iron based materials have shown much promise and due to their magnetic properties have been the focus of much research.

In recent studies, magnetite (Fe_3O_4) has shown much promise in being able to remove both As(III) and As(V) from aqueous solution [3]. Luther et al., showed that Fe_3O_4 had a capacity of 8.2 mg/g and 5.6 mg/g for As(III) with 1 hour and 24 hour contact times, respectively [3]. The binding capacity for As(V) with the Fe_3O_4 nanomaterial was found to be 6.7 mg/g and 4.7 mg/g for the one hour and 24 hour contact times, respectively [3]. Makris et al. found that Fe based water treatment residuals showed a high affinity for the binding of both As(III) and As(V) with capacities up to 15 mg/kg [26]. Garcia et al., extended this study to include mixtures of Fe_3O_4, $MnFe_2O_4$, and Mn_3O_4 nanomaterials [18]. The binding capacity of As(III) to the different mixtures: the pure Fe_3O_4 showed a binding capacity of 17.1 mg/g; the 25% Mn into the Fe_3O_4 lattice showed a slight increase in the binding capacity for to 23.8 mg/g; the 50% substituted showed the maximum binding capacity of 41.5 mg/g; the 75% Mn substituted Fe_3O_4 capacity was 16.7mg/g; and the pure Mn_3O_4 had a binding capacity of 13.5 mg/g. The As(V) binding capacities for the same materials was determined to 7.0 mg/g, 7.9 mg/g, 13.9 mg/g, 8.2 mg/g, and 7.5 mg/g for the Fe_3O_4, 25% Mn:Fe, 50% Mn:Fe, 75% Mn:Fe, and the pure Mn_3O_4 nanomaterials,

respectively. The manganese studies raise some concern as manganese is potentially an endocrine disrupting chemical and it has been shown that manganese oxides undergo reductive dissolution in reaction with arsenic [27].

Alternatively, iron sulfides have shown promising results for removing arsenic. For example, the interaction of pyrite (FeS_2) with As shows surface reactions between arsenic and pyrite to produce arsenian pyrite ($Fe(SAs)_2$) and arsenopyrite (FeAsS). The aforementioned products precipitate under most reducing conditions and are stable. Another benefit witnessed in pyrite nanofiltration is the stabilization of arsenic contaminated soil and sediments [9]. Since arsenic adsorption in anoxic environments strongly correlates with formation of iron sulfide minerals, such as pyrite, much research has gone into iron derivatives' application as a material to remove arsenic in anoxic environments. However, research has shown that the efficiency of the removal of arsenic depends on factors such as particle size, time, interferences, pH, temperature, and the oxidation state of the arsenic. Results from particle size studies have revealed a 200 fold increase in the adsorption of arsenic by pyrite nanoparticles when the particle size of pyrite was decreased from 300nm to 12nm [10]. Previously investigated reactions have shown that the concentration of As (III) was directly proportional to pH with optimum binding at the pH range of 7–10. However, the optimum binding for As (V) occurred in a pH range of 4–6 with moderate to high levels of irreversibility [9]. Compared iron oxide based materials; it was found that As (III) had a higher binding affinity to iron sulfides than As (V) [3]. Greigite (Fe_3S_4) is; quite similar to magnetite in which both compounds share the same amount of atoms and similar properties, both are magnetic, and may provide a higher binding affinity and capacity for As(III) and As(V) [13]. Another Iron sulfide which has ferromagnetic properties is pyrrhotite (Fe_7S_8), which is stable and easily synthesized [28].

In the present study, pyrrhotite, (Fe_7S_8), was synthesized and utilized for the removal of arsenite and arsenate from aqueous solutions. The nanoparticles were synthesized by mixing 30mM iron (III) chloride hexa-hydrate and 60mM thiourea in a mixture of ethylene glycol H_2O; the mixture was then autoclaved at high temperatures. The synthesized materials were characterized using X-Ray Diffraction which showed the correct phase with an average particle size of 29.86 ± 0.87nm. Studies were performed to determine the effect of pH, time, temperature, binding capacity, the kinetics, and thermodynamics of the binding process. As well studies were performed to observe the effects of potentially interfering anions naturally found in water on the arsenic binding process.

2. Experimental

2.1 Synthesis of the nanomaterial

Solvothermal synthesis of the pyrrhotite (Fe_7S_8) nanomaterial was performed using a synthesis method similar to Zhang and Chen [29]. In brief the synthesis of the Fe_7S_8 nanomaterial was performed using 30mmol of iron(III) chloride ($FeCl_3{\cdot}6H_2O$, Acros Organics) and 60mmol of thiourea (Acros Organics) dissolved in a mixture of 60mL of ethylene glycol (Acros Organics) and 20mL of Millipore water. The resulting solution was added to Teflon lined autoclaves at approximately 80% of the total volume capacity. The autoclaves were sealed, placed in an oven, and reacted at 180 °C for 1 h. Subsequent to the

reaction the autoclaves were cooled naturally to room temperature and filtered using a Buchner funnel. The filtered nanomaterial was then washed with acetone and methanol to remove any contaminants/byproducts formed during the reaction.

2.2 X-Ray Diffraction analysis

The X-ray diffraction analysis of the Fe_7S_8 nanoparticles was performed using a Rigaku Miniflex Diffractometer. The Fe_7S_8, NPs were ground to a fine powder with a mortar and pestle and placed in to a sample holder. The XRD patterns were collected using the following conditions a start angle of 20° and stop angle of 60° in a step width of 0.05° in 2θ, and a counting time of 5s. The average grain size of the nanomaterials was determined using Scherrer's equation and a Gaussian fitting of three independent diffraction peaks. The fitting of the X-ray diffraction pattern were performed using a Le Bail fitting procedure with fixed intensities of the diffraction lines in the FullProf 2001 Suite of programs and crystallographic data from the literature [30].

2.3 SEM

SEM was performed using a Zeiss LS10 EVOSEM microscope with a working voltage of 20 kV, an operating current of 2.5 A, and a working distances of 6.0 mm and 4.5 mm for the low and high magnification pictures, respectively. In addition, the samples were sputter coated using an Au target to enhance sample conductivity.

2.4 pH profile

The binding of As (III) and As (V) to Fe_7S_8 nanoparticles was investigated from pH 2 to 6 using 300 ppb solutions. pH adjustment of the 300 ppb solutions of both As (III) and As (V) was performed using either diluted nitric acid or sodium hydroxide. All reactions were performed in triplicate for statistical purposes. Aliquots consisting of 4.0 mL of the pH adjusted 300 ppb solutions of As (III) or As (V) were transferred into 5 mL polyethylene test tubes, which contained 10 mg of the dried nanomaterial. The solutions and nanomaterials were equilibrated on a rocker at room temperature for 1 h. In addition, control samples containing only the pH-adjusted solutions of either As (III) or As (V) ions were also reacted in triplicate, for statistical purposes. Subsequent to equilibration, the samples and controls were centrifuged at 3500 rpm for 15 min and the supernatant was saved for analysis using a Perkin Elmer AAnalyst 800 (Perkin Elmer, Shelton, CT) operated in GFAAS mode, for the determination of the amount of arsenic remaining in the solution.

2.5 Time dependency

Time dependency studies were performed similarly to the pH study to determine the minimum time required for the binding of both the As (III) and As (V) ions to the Fe_7S_8 nanomaterial. Solutions consisting of As (III) or As (V) at 300ppb, pH adjusted to 4 were reacted with 10mg of Fe_3S_4 at various time intervals. Aliquots consisting of 4 mL of either As (III) or As (V) were equilibrated at room temperature on a rocker for 5, 10, 15, 20, 30, 60, 90, 120, and 240 min with the nanomaterials. Again control samples consisting of only the As (III) and As (V) solutions were used as controls and treated the same as the reaction samples. All of the reaction and control samples were performed in triplicate for statistical

purposes. After equilibration, the samples and control samples were centrifuged at 3500 rpm for 15 min and the supernatants were stored for GFAAS analysis.

2.6 Thermodynamic studies

Thermodynamics studies were conducted to determine the ΔG, ΔH, and the ΔS for the binding of both As (III) and As (V) binding to the Fe_7S_8 nanomaterial. The thermodynamic studies were performed using a total As concentration of 300 ppb. The pH of the solutions was adjusted to the previously determined optimum binding pH of 4. Aliquots consisting of 4.0 mL of the solutions were added reaction tubes containing 10 mg of Fe_3S_4, and equilibrated for 1 hour on a rocker at varying temperatures of 4°C, 21°C, and 45°C. In addition, control solutions consisting of the arsenic solutions without the nanomaterials were also made and treated the same as the reaction samples. All reaction and controls samples were performed in triplicate for statistical purposes. After equilibration, the samples were centrifuged at 3500 rpm for 15 min and the supernatants saved for analysis using GFAAS.

2.7 Kinetic studies

Studies were performed using 300 ppb of either As (III) or As (V) at different time intervals and temperatures, to better understand the mechanisms of binding. The pH of the solutions was adjusted to a pH of 4 using either dilute nitric acid or dilute sodium hydroxide. Aliquots of 4.0 mL of the solutions were added to the test tubes containing 10 mg of Fe_3S_4. The samples were equilibrated on rockers at varying temperatures of 4°C, 21°C, and 45°C at the following time intervals 5, 10, 15, 20, 30, 60, 90, 120, and 240 min. In addition, control solutions consisting of only the As(III) or As(V) were treated the same as the reaction samples. Subsequent to equilibration the samples and controls were centrifuged at 3500 rpm for 15 minutes and the supernatants were stored for GFAAS analysis. Furthermore, the samples and the control samples were prepared and analyzed in triplicate for statistical purpose.

2.8 Activation energy studies

The kinetic data allowed for the determination of the activation energy (E_a) of the binding of both As(III) and As(V) to the Fe_7S_8. An Arrhenius plot was constructed by plotting the Ln k (rate constant) against 1/T (in kelvin). The linearized form of the Arrhenius equation is given below in Eq. (1):

$$Ln(k)=\frac{E_a}{R}\frac{1}{T}+Ln(A) \quad (1)$$

where k is the rate constant for the reaction at a given temperature, E_a is the activation energy for the process, R is the gas constant (8.314), T is the temperature given in Kelvin, and A is the frequency factor for a given reaction.

2.9 Interference studies

The binding of the As(III) and As(V) ions in the presence of various common anions was performed as possible interferences to the binding process was investigated. The interference studies consisted of performing reactions with various concentrations of Cl^-, NO_3^-, SO_4^{2-},

and PO_4^{3-} added to 300ppb solutions of either As (III) or As (V) and pH adjusted to 4. Aliquots consisting of 4.0mL of a solution containing 300ppb and either 1000, 100, 30, 3, or .3ppm of the possible interfering ion were reacted with 10mg of Fe_7S_8 and equilibrated on a rocker for 1 h at room temperature. The reaction controls consisted of either the As(III) or As(V) with the possible interfering ions present in the solution without the nanomaterial. After the reaction was complete, the samples and controls were centrifuged at 3500 rpm for 5min and the supernatants were saved for analysis by GFAAS. All reactions and controls were conducted in triplicate.

2.10 Capacity studies

Capacity studies were performed using various concentrations of As (III) and As (V), using an isotherm model to determine the binding capacity of the nanomaterial. The concentrations consisted of 3, 30, 100, 300, and 1000 ppm of either As (III) or As (V). The solutions were then added to test tubes containing 10 mg of pyrrhotite (Fe_7S_8). Each concentration was performed in triplicate and the controls reactions consisting of only the arsenic solutions were prepared and treated same as the samples. The solutions were equilibrated on a rocker for 1 hr subsequently centrifuged at 3500 rpm for 15 minutes. The supernatants were then decanted and saved for analysis using ICP-OES.

2.11 GFAAS analysis

Supernatants collected from the pH profile, interference studies, thermodynamic, time dependency, and kinetic studies were analyzed using a Perkin Elmer AAnalyst 800 atomic absorption spectrometer with Winlab32 software. The operational parameters of the GFAAS are presented in Table 1. All sample determinations were obtained from calibration curves with R^2 values of 0.99 or better.

2.12 ICP-OES analysis

A Perkin Elmer Optima 8300 ICP-OES (Perkin Elmer, Shelton CT) with the Winlab 32 software. The operational parameters of the ICP-OES are presented in Table 2. All samples were diluted to fit within the values used for the calibration of the instrument. All of the As concentrations were obtained from calibration curves with R^2 value of 0.99 or better.

2 Discussion

3.1 X-Ray Diffraction

As can be seen in Fig. 1 the X-ray diffraction pattern was determined to consist of a mixture of two phases; the primary phase was determined to be Fe_7S_8 or pyrrhotite and the minor phase was determined to have been Fe_3S_4 (greigite). The pyrrhotite phase was determined to be approximately 90% of the mixture and the greigite phase was the remaining 10%. Based on the calculated composition of the two phases present in the sample the observed binding in the sample will be attributed to the Fe_7S_8 phase. The refined parameters for the Fe_7S_8 phase was in a monoclinic space group C2/C with the following lattice parameters a= 12.00185 Å, b= 6.88438 Å, c= 13.18790 Å, with $\alpha = \gamma = 90$ and $\beta = 119.419$, which matched close to the literature values [31]. The refined parameters for the Fe_3S_4 phase was determined to be in a cubic with space group F D 3 M with the following lattice parameters

a=b=c= 9.96841Å and α= β=γ= 90, which were found to follow very closely to the literature values [32]. The overall X^2 for the fitting was determined to be 0.611 showing an excellent agreement between the fitting and the experimental data. The respective Bragg peaks for each of the phases are shown at the bottom of the diffraction pattern. The Bragg peaks for the Fe_7S_8 phase are the higher Bragg peaks where are the Fe_3S_4 peaks are the lower Bragg peaks. Furthermore, the average grain size for the Fe_7S_8 phase was determined to be 23.3 nm based on the 023 (35.04°) diffraction peak. The greigite phase was determined to have an average grain size of 18.7 nm, based on the 400 (36.04°) diffraction peak. All other diffraction peaks for the phases were either multiple diffraction peaks from both phase or were multiple peaks from an individual phase.

3.2 SEM

Fig. 2 shows the SEM images of the synthesized Fe_7S_8 material which consists of rag-like sheets/platelets, spherical particles and some irregular, and some rod shaped particles, consisting of various shapes and sizes. The particles were somewhat clustered, which was due to the lack of using a surfactant to stabilize the particles during the synthesis. Upon closer inspection (Figure 2 B) the larger clusters are composed of smaller particles approximately 30 nm diameters. Surfactants were not used during the synthesis process to provide a clean metal sulfide surface for the reaction to occur to study the interaction of the As(III) and As(V) ions.

3.3 pH studies

Fig. 3 shows the binding of As(III) and As(V) to Fe_7S_8 from a pH 2 to pH 6, respectively. As can be seen in Fig. 3, the binding of As(III) at pH 2 was approximately 51% and increased to approximately 100% at pH 3, the binding of the As(III) remained thereafter. On the other hand, the binding of As(V) was unaffected with changes in pH. As (V) binding remained constant between 90–99% bound across the pH range of interest. From the results, it was observed that the percent binding had stabilized from pH 4 to pH 6; pH 4 was then selected as the optimal binding pH for all further studies. The pH profile studies are in agreement with, other studies in the literature for arsenic binding to other metal sulfides/oxides nanomaterials [8–18]. For example, FeS_2 nano-adsorbents have shown a similar trend in binding, the higher the pH the higher the amount of As bound. Some other examples with similar trends include FeS, Fe_2O_3, and Fe_3O_4. A study conducted by Garcia et al. showed the adsorption of As (III) and As (V) to Fe_3O_4 and Mn_3O_4. In the study, the binding of As (III) and As (V) to Fe_3O_4 was observed to not be pH dependent. However, the adsorption of As to pure Mn_3O_4 was observed to decrease as the pH increased; which was attributed Mn_3O_4 having a PZC around 4.5, which would decrease the binding of with the ions [15]. FeS (macanite), has been shown to have a $pH_{i.e.p}$ or PZC of approximately 3.5, which would show similar behavior to the Mn_3O_4 nanomaterials and similar binding was observed in the current study [33].

3.4 Time dependency studies

The binding of the arsenic ions to Fe_7S_8 nanomaterials as a function of time is shown in Fig. 4. As can be seen in Fig. 4, the binding of As (III) to Fe_7S_8 occurred within the first 5 minutes with 90% of the total As bound and a slight increased to 99% at the 60 minute

contact time. The binding remained relatively constant afterwards up to a contact time of 240 minutes. A similar trend was observed for As (V), within the first 5 minutes, approximately 90% of As(III) had bound to the nanomaterial and minor increase of 10% of arsenic binding occurred throughout the study. A direct relationship was observed between the arsenic ions and the time the samples were equilibrated. These binding trends have been observed in the literature for the binding of As(III) and As(V) to various transition metal oxide nanomaterials [3, 11,13,15–18].

3.5 Kinetics Studies

The kinetics data are shown in Fig. 5 and was found to plot a straight line using a plot of the adsorption of arsenic (Q_t) against time. The plot of the adsorption of the arsenic against time giving a straight line indicates a zero order reaction was occurring between the adsorbent and the arsenic ions, within the first 20 minutes of contact. After the first 20 minutes of contact the adsorption of metal ions per g of nanomaterial was not changing, as was observed in the time dependency studies. A zero order reaction would be indicative of a ligand exchange or an ion exchange reaction. The rate constants were determined and are shown in Fig. 4. According to the results the rate constants, k, increases as temperature increases indicating an endothermic reaction was occurring for the binding of both the As (III) and As (V) to the Fe_7S_8 nanomaterial. Lien et al showed that the kinetics of adsorption can follow zero order at low concentrations between arsenite and zero-valent iron nanoparticles [34].

3.6 Capacity studies

The results from the capacity studies are shown in Table 3 for 1 h contact time for As(III) and As(V) binding to Fe_7S_8 nanomaterial. The capacity studies were conducted at room temperature (25°C). Both As(III) and As(V) binding to the nanomaterial was determined to follow the Langmuir isotherm model and were fitted using the Langmuir isotherm equation. The correlation coefficients for the linear fittings of the data shown in Table 3 are 0.99 or better (R^2). The data present in Table 4 shows high binding capacities of the Fe_7S_8 nanomaterial for both As(III) and As(V) at a pH of 4. From the present study, As (V) showed a higher binding capacity to the nanomaterial than As (III). The As(V) binding capacity was approximately 2 times the binding capacity observed for the As(III). The observed As(III) binding capacity was 14.3 mg/g and the As(V) binding capacity was 31.3 mg/g within 1 h of contact time.

In recent studies, the adsorption of arsenic to different metal oxide nanoparticles was within the range of the present study, where the absorption capacity for As(III) was 2–30 mg/g and for As(V) it was 3–30 mg/g [3,11,14,15,17,26]. Whereas FeOOH (Goethite) has been shown to have capacities of 11.2 and 12.2 mg/g for the binding of As(III) and As(V), respectively [22]. In addition, manganese oxides have shown to capacities in the same rages as the Fe_7S_8 in the current study (15). Mn_3O_4 has been shown to have binding capacities of around 7.0 and 13.5 mg/g for As(V) and As(III), respectively [15]. Another example, of a materials with a similar binding capacity is titanium dioxide in the anatase form has a capacity of 30.5 mg/g for As(V) and a capacity of 30.0 mg/g for As(III) [17]. The capacity of titanium dioxide changes with respect to its particle size, where the smaller the particle size, the

higher the capacity of the nanomaterial. In addition, FeS has shown low binding capacities for As(III) of approximately 1.05 mg/g where as FeS_2 has shown binding capacitie of 17.3 mg/g, which is comparable to the Fe_7S_8 in the current study [35]. Similarity on iron sulfide coated sand binding capacities of 41.7 mg/g were observed and binding capacities of 137.0 mg/g have been observed at a pH 5.0 [36].

3.7 Interferences studies

Fig. 6–9 show the results from the individual interference studies for chloride, nitrate, sulfate, and phosphate, respectively, while Fig. 10 shows the results for the combined interferences and its effects on the binding of arsenite and arsenate. As can be seen in Fig. 6, the adsorption of As(III) and As(V) to Fe_7S_8 in the presence of the Cl^- anion remained unaffected throughout the analysis in which the binding of arsenic increased as the concentration of Clincreased. Fig. 7 shows the effect of the NO_3^- anion on the binding of arsenic to pyrrhotite. It can be seen NO_3^- had little to no effect on the adsorption of As(III) to the Fe_7S_8 nanomaterial remaining above an 85% binding. On the other hand, the adsorption of As(V) to Fe_7S_8 slightly increased as the concentration of NO_3^- increased.

As can be seen in Fig. 8, the SO_4^{2-} had little to no effect on the binding of As (III) and As (V) to Fe_7S_8 in which the percent of arsenic bound to the nanomaterial remained constant at 100% however in the presence of 1000 ppm of SO_4^{2-}, the percent binding of As (III) dropped to approximately 95%. Fig. 9 shows the effect of PO_4^{3-} on the binding of arsenic to Fe_7S_8. In the present study, the data shows that at low concentrations of PO_4^{3-} the binding of As (III) and As (V) to Fe_7S_8 was unaffected remaining above 80 % binding. However, as the concentration of the PO_4^{3-} anion increased, the percent bound of As (III) and As (V) decreased until the concentration of PO_4^{3-} reached 1000 ppm in which the percent binding of As(III) and As(V) to the nanomaterial decreased to approximately 55% and 35 %, respectively.

The combined interference study, refer to Fig. 10, showed that the of binding of As(III) was generally unaffected by the presence of the combination of Cl^-, NO_3^-, SO_4^{2-}, and PO_4^{3-} in solution; except when the concentration of each of the anions was 1000 ppm in the combined interference study where percent binding of As(III) was observed to decrease by approximately 10%. On the other hand, the binding of As(V) was unaffected throughout the study, where it remained at 100% bound to the nanomaterial. Throughout the individual interference studies, there was little to no effect on the adsorption of As(III) and As(V) with the exception of the PO_4^{3-} anion where it greatly affected the of As(V) at high concentrations. The combined interference studies, again, had small effects on the binding of As(III) but did not affect the adsorption of As(V) to Fe_7S_8. The lack of observed reduction in the binding of the As(III) and As(V) in the presence of all the interfering ions maybe a synergistic effect of all the ions in solution. The interferences may actually be interfering with each other in solution and not affect the arsenic ions and may actually enhance the arsenic binding. In other studies investigating the binding of As(III) and As(V) to different nanomaterials PO_4^{3-} has been shown to be the largest interference on the binding process [3, 11, 14,15, 17, 23–25]. In addition, the other interferences investigated in the present study behaved similarly with the binding of arsenic to oxide materials [3, 11, 14, 15, 17,].

3.8 Thermodynamic studies

The data obtained from the thermodynamic studies was used to determine Gibbs free energy, entropy, and the enthalpy in the system are shown in Table 4. The change in the Gibbs free energy was calculated for both As(III) and As(V) at various temperatures. The relationship between ΔG, ΔH, and ΔS and the relationship between ΔG and the Ln K_d are shown in equations 2 and 3, respectively.

$$\Delta G = -RTLn(k_d) \quad (2)$$

$$Ln(k_d) = \frac{\Delta S}{R} - \frac{\Delta H}{RT} \quad (3)$$

In which ΔG is the change in Gibbs free energy; R is the gas constant (8.314 $J \cdot K^{-1} \cdot mol^{-1}$); T is the absolute temperature in Kelvin; K_d is the distribution coefficient; ΔS is the change in entropy; ΔH is the change in enthalpy. By plotting the Ln K_d against 1/T (in K) the ΔH of the reaction can be determined from the slope of the line and from the intercept of the plot the ΔS can be determined, as shown in Fig. 10. The calculated thermodynamic parameters are shown in Table 4. According to the results, the binding system gets less spontaneous as the temperature increases, which does not correlate to previous studies involving the adsorption of arsenic with metal sulfides and metal oxides [12–14]. For example, A. Goswami et al. studied the adsorption of arsenic to copper (II) oxide. From the study, the ΔG for the sorption process was between −16.07 and −5.48 kJ/mol and was temperature dependent [13]. In the present study, ΔG the sorption process was 7.95 kJ/mol (277 K), 6.73 kJ/mol (295 K), and 4.71 kJ/mol (318 K) for As (III) and 6.12 kJ/mol (277 K), 4.62 kJ/mol (295 K), and 0.80 kJ/mol (318 K). The ΔG values obtained in the current study are small and close to zero indicating the reaction are also in equilibrium. Goswami et al. observed a similar relationship between ΔG and the reaction temperature, where the change in ΔG becomes smaller with an increase in temperature indicating an endothermic reaction was occurring [13, 37]. The adsorption Pb^{2+} with phosphate modified kaolinite clays also showed an endothermic reaction, the ΔG decreases with increasing temperature [37].

The ΔH and ΔS were both determined by plotting Ln K_d against 1/T (in K) from the plot ΔH was determined from the slope of the line and the ΔS was determined from the intercept of the plot. Fig. 12 shows the thermodynamic plot at three different temperatures (277, 298, and 318 K) for the binding of both As(III) and As(V) to the nanoparticles. The ΔH and ΔS values for the binding of arsenic to the Fe_7S_8 nanoparticles are presented in Table 4. The values for the enthalpy indicate that the process for the binding of arsenic was endothermic confirming the results of the type of reaction obtained from the Gibbs free energy studies. Furthermore, the binding of As(III) had a much larger ΔH than the binding of As(III), where As(V) had a ΔH of 27.2 kJ/mol while As(III) had a ΔH of 42.5 kJ/mol indicating that the binding of As(V) is less more endothermic than As(III) binding. However these values for the enthalpy of binding indicate that the reaction occurs through different process for the arsenic(III) and arsenic(V). The binding of arsenic(III) occurs through physisorption as indicated through the enthalpy of binding being less than 40 kJ/mol [38]. Whereas the

enthalpy of binding for the arsenic(V) indicate that the reaction occurs through chemisorption because the enthalpy of binding is greater than 40kJ/mol [38]. However, the ΔH arsenic(V) is only 7 kJ/mol over the energy for chemisorption, so the process for As(V) binding maybe a combination of both sorption types. On the other hand, the ΔS for the binding of both As(III) and As(V) were both positive values indicating an increase in the entropy of the system after binding. The increase in the entropy of binding is linked to the release of ions from the surface of the nanomaterials, and to disruption in the water molecules surrounding the particles and ions after binding occurs. The data also indicates that the binding of the arsenic(V) to the nanomaterial is more favorable as the entropy of the system increase by almost double that observed with arsenic(III) binding. The different binding mechanisms observed for both the arsenic(III) and arsenic(V) help to explain why the ions have different binding capacities.

The data from the activation energy studies indicate that the energy required for the binding to occur are very close arsenic(III) and arsenic(V). The arsenic(III) ions require approximately 5 kJ/mol of energy for the binding to occur over the arsenic(V), as can be seen in Table 4. The similarities in the activation energies indicates that arsenic(III) is slightly less favorable than As(V). In other words more energy is required to start the binding process than arsenic(V),but also may be indicating both ions go through the physisorption. The binding of cadmium(II) ions to pyrite had activation energy of 12.09 kJ/mol which is in the range of the activation energies observed in the present study, which suggest that chemisorption is the driving force of the adsorption [39]. The activation energy for the binding process of chemisorption has also been shown to range from 8 to 80 kJ/mol [40]. The less favorable binding of arsenic(III) to the nanomaterials was also expressed through the adsorption capacities, arsenic(III) was lower by approximately a factor of two. The combination of energy differences in the energy of binding, the differences in the enthalpy of binding, and the difference in the entropy increase, all suggest that the binding of arsenic(III) is less favorable to the Fe_7S_8 nanomaterials and thus would have a lower binding capacity compared to arsenic(V).

4 Conclusions

The binding of As(III) and As(V) to the Fe_7S_8 was determined to be almost pH independent… The As(III) had low binding at pH 2 and increased dramatically to pH 3 to approximately 100%. Binding of both As(III) and As(V) ions was found to occur with the first 20 minutes of contact with the Fe_7S_8 nanomaterial and remained constant thereafter. The binding of both As(III) and As(V) was determined to follow zero kinetics, which was more than likely due to the low concentrations and the ratio of adsorption sides to ions. The arsenic was found to be endothermic the ΔG for the binding of both As ions was slightly positive, but the ΔG were close to zero indicating that the reaction was very close to equilibrium. The ΔS was shown to increase with the binding. Whereas the ΔH and the E_a indicated that the binding of As(III) was occurring through chemisorption. The ΔH and the E_a for the binding of the As(V) indicated that the binding may be occurring through a combination of both chemisorption and physisorption. The As(V) showed a binding capacity approximately twice that of the As(III), which were 31.3 and 14.3 mg/g, respectively.

Acknowledgments

Authors would like to thank the NIH UTPA RISE program (Grant Number 1R25GM100866-03). The Authors acknowledge financial support from the Welch Foundation for supporting the Department of Chemistry (Grant number GB-0017).

References

1. Masscheleyn PH, Delaune RD, Patrick WH Jr. Effect of redox potential and pH on arsenic speciation and solubility in a contaminated soil. Environ. Sci. Technol. 1991; 25:1414–1419.
2. Edenborn HM, Belzile N, Mucci A, Lebel J, Silverberg N. Observations on the diagenetic behavior of arsenic in a deep coastal sediment. Biogeochem. 1986; 2:359–376.
3. Luther S, Borgfeld N, Kim J, Parsons JG. Removal of arsenic from aqueous solution: A study of the effects of pH and interfering ions using iron oxide nanomaterials. Microchem. J. 2012; 101:30–36. (2012).
4. Sun HJ, Rathinasabapathi B, Wu B, Luo J, Pu LP, Ma LQ. Arsenic and selenium toxicity and their interactive effects in humans. Environ. Int. 2014; 69:148–158. (2014). [PubMed: 24853282]
5. O'Day PA, Vlassopoulos D, Root R, Rivera N. The influence of sulfur and iron on dissolved arsenic concentrations in the shallow subsurface under changing redox conditions. Proc. Natl Acad. Sci. U.S.A. 2004; 101:13703–13708. [PubMed: 15356340]
6. Bhowmick S, Chakraborty S, Mondal P, Van Renterghem W, Van den Berghe S, Roman-Ross G, Iglesias M M. Montmorillonite-supported nanoscale zero-valent iron for removal of arsenic from aqueous solution: Kinetics and mechanism. Chem. Eng. J. 2014; 243:14–23. (2014).
7. Zouboulis AI, Kydros KA, Matis KA. Removal of hexavalent chromium anions from solutions by pyrite fines. Water Res. 1995; 29:1755–1760.
8. Bostick BC, Fendorf S. Arsenite sorption on troilite (FeS) and pyrite (FeS2). Geochimi. Cosmochim. Acta. 2003; 67:909–921.
9. Bulut G, Yenial Ü, Emiroglu E, Sirkeci AA. Arsenic removal from aqueous solution using pyrite. Journal of Cleaner Production. 2014; 84:526–532.
10. Han DS, Song JK, Batchelor B, Abdel-Wahab A. Removal of arsenite (As (III)) and arsenate (As (V)) by synthetic pyrite (FeS2): synthesis, effect of contact time, and sorption/desorption envelopes. J. Colloid Interface Sci. 2013; 392:311. [PubMed: 23195771]
11. Parsons JG, Lopez ML, Peralta-Videa JR, Gardea-Torresdey JL. Determination of arsenic(III) and arsenic(V) binding to microwave assisted hydrothermal synthetically prepared Fe_3O_4, Mn_3O_4, and $MnFe_2O_4$ nanoadsorbents. Microchem. J. 2009; 91:100–106. (2009).
12. Kong S, Wang Y, Hu Q, Olusegun AK. Magnetic nanoscale Fe–Mn binary oxides loaded zeolite for arsenic removal from synthetic groundwater. Colloids Surf., A. 2014; 457:220–227.
13. Goswami A, Raul PK, Purkait MK. Arsenic adsorption using copper (II) oxide nanoparticles. Chem. Eng. Res. and Des. 2012; 90:1387–1396.
14. Mamindy-Pajany Y, Hurel C, Marmier N, Roméo M. Arsenic (V) adsorption from aqueous solution onto goethite, hematite, magnetite and zero-valent iron: Effects of pH, concentration and reversibility. Desalination. 2011; 281:93–99.
15. Garcia S, Sardar S, Maldonado S, Garcia V, Tamez C, Parsons JG. Study of As(III) and As(V) oxoanion adsorption onto single and mixed ferrite and hausmannite nanomaterials. Microchem. J. 2014; 117:52–60. [PubMed: 25097269]
16. Guana X, Dub J, Mengc X, Suna Y, Sunc B, Hu Q. Application of titanium dioxide in arsenic removal from water: A review. J. Hazard. Mater. 2012; 215–216:1–16.
17. Wen Z, Zhang Y, Dai C, Chen B, Guo S, Yu H, Wu D. Synthesis of ordered mesoporous iron manganese bimetal oxides for arsenic removal from aqueous solutions. Microporous and Mesoporous Mater. 2014; 200:235–244.
18. Lunge S, Singh S, Sinha A. Magnetic iron oxide (Fe_3O_4) nanoparticles from tea waste for arsenic removal. J. Magn. Magn. Mater. 2014; 356:21–31.

19. Guptaa K, Bhattacharyab S, Chattopadhyayc D, Mukhopadhyayb A, Biswasd H, Duttad J, Rayd NR, Ghosh UC. Ceria associated manganese oxide nanoparticles: Synthesis, characterization and arsenic(V) sorption behavior. Chem. Eng. J. 2011; 172:219–229.
20. Guo X, Du Y, Chen F, Park H-S, Xie Y. Mechanism of removal of arsenic by bead cellulose loaded with iron oxyhydroxide (β-FeOOH): EXAFS study. J. Colloid Interface Sci. 2007; 314:427–433. [PubMed: 17604042]
21. Zhao Z, Jia Y, Xu L, Zhao S. Adsorption and heterogeneous oxidation of As(III) on ferrihydrite. Water Res. 2011; 45:6496–6504. [PubMed: 22000059]
22. Guo H, Ren Y, Liu Q, Zhao K, Li Y. Enhancement of arsenic adsorption during mineral transformation from siderite to goethite: mechanism and application. Environ. Sci. Technol. 2013; 47:1009–1016. [PubMed: 23252340]
23. Gao Y, Mucci A. Individual and competitive adsorption of phosphate and arsenate on goethite in artificial seawater. Chem. Geol. 2003; 199:91–109.
24. Chunming S, Puls RW. Arsenate and arsenite removal by zerovalent iron: effects of phosphate, silicate, carbonate, borate, sulfate, chromate, molybdate, and nitrate, relative to chloride. Environ. Sci. Technol. 2001; 35:4562–4568. [PubMed: 11757617]
25. Hongshao Z, Stanforth R. Competitive adsorption of phosphate and arsenate on goethite. Environ. Sci. Technol. 2001; 35:4753–4757. [PubMed: 11775149]
26. Makris KC, Sarkar D, Datta R. Evaluating a drinking-water waste by-product as a novel sorbent for arsenic. Chemosphere. 2006; 64:730–741. [PubMed: 16405955]
27. Katsoyiannis IA, Zouboulis AI, Jekel M. Kinetics of bacterial As(III) oxidation and subsequent As(V) removal by sorption onto biogenic manganese oxides during groundwater treatment. Ind. Eng. Chem. Res. 2004; 43:486–493.
28. Powell AV, Vaqueiro P, Knight KS, Chapon LC, Sánchez RD. Structure and magnetism in synthetic pyrrhotite Fe_7S_8: A powder neutron-diffraction study. Phys. Rev. B. 2004; 70:014415.
29. Zhang ZJ, Chen XY. Magnetic greigite (Fe_3S_4) nanomaterials: Shape-controlled solvothermal synthesis and their calcination conversion into hematite (α-Fe_2O_3) nanomaterials. J. Alloys Compd. 2009; 488:339–345.
30. LeBail A, Duroy H, Fourquet JL. Ab-initio structure determination of $LiSbWO_8$ by Xray powder diffraction. Mater. Res. Bull. 1988; 23:447–452.
31. Tokonami M, Nishiguchi K, Morimoto N. Crystal structure of a monoclinic pyrrhotite (Fe7S8). American Mineralogist. 1972; 57:1066–1080.
32. Skinner BJ, Erd RC, Grimaldi FS. Greigite, the thio-spinel of iron: a new mineral. American Mineralogist. 1964; 49:543–555.
33. Bebie J, Schoonen MAA, Fuhrmann M, Strongin DR. Surface charge development on transition metal sulfides: An electrokinetic study. Geochim. Cosmochim. Acta. 1998; 62:633–642.
34. Lien HL, Wilkin RT. High-level arsenite removal from groundwater by zero-valent iron. Chemosphere. 2005; 59:377–386. [PubMed: 15763090]
35. Bostick BC, Fendorf S. Arsenite sorption on troilite (FeS) and pyrite (FeS2). Geochimica et Cosmochimica Acta. 2003; 67:67, 909–921.
36. Han YS, Gallegos TJ, Demond AH, Hayes KF. FeS-coated sand for removal of arsenic(III) under anaerobic conditions in permeable reactive barriers. Water Res. 2011; 45:593–604. [PubMed: 20974481]
37. Unuabonah EI, Adebowale * KO, Olu-Owolabi BI. Kinetic and thermodynamic studies of the adsorption of lead (II) ions onto phosphate-modified kaolinite clay. Journal of Hazardous Materials. 2007; 144:386–395. [PubMed: 17156914]
38. Din, Muhammad Imran; Mirza, Muhammad Latif; Ata, Sadia; Athar, Makshoof; Mohsin, Ul Ijaz. Thermodynamics of Biosorption for Removal of Co(II) Ions by an Efficient and Ecofriendly Biosorbent (Saccharum bengalense): Kinetics and Isotherm Modeling. J. Chem. 2013; 2013:1–11.
39. Boparai HK, Joseph M, O'Carroll DM. Kinetics and thermodynamics of cadmium ion removal by adsorption onto nano zerovalent iron particles. J. Hazard. Mater. 2011; 186:458–465. [PubMed: 21130566]

40. Mahmood T, Saddique MT, Naeem A, Mustafa S, Zeb N, Shah KH, Waseem M. Kinetic and thermodynamic study of Cd(II), Co(II) and Zn(II) adsorption from aqueous solution by NiO. Chem. Eng. J. 2011; 171:935–940.

Highlights

As(III) and As(V) binding was pH independent.

As(III) and As(V) adsorption was zero order and exothermic

Fe_7S_8 had a lower binding capacity for As(III) than As(V)

Activation energy of the binding process was higher for As(III) than As(V)

PO_4^{3-} interfered with As binding whereas Cl^-, NO_3^-, and SO_4^{2-} had no effect

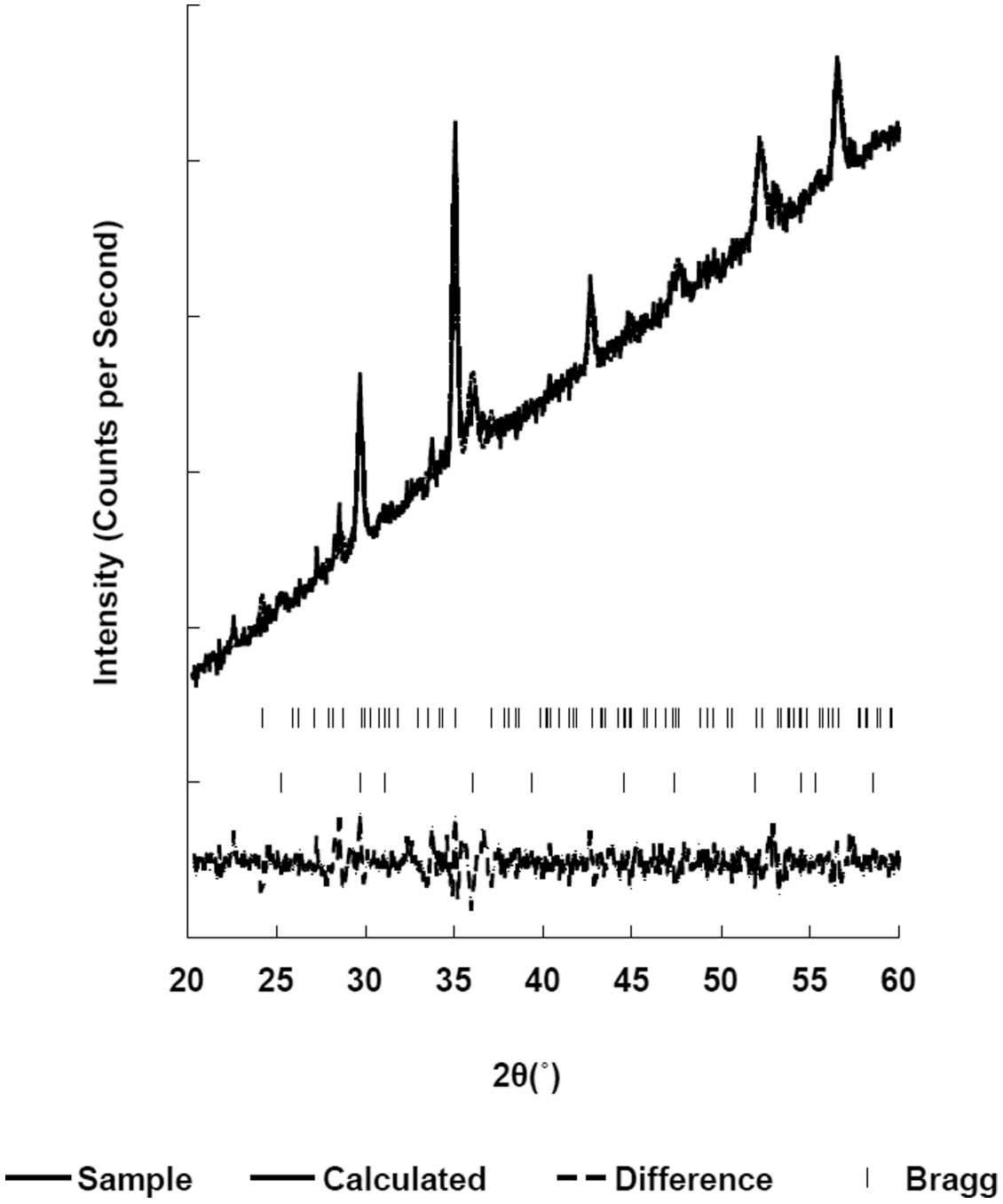

Figure 1.
Powder X-ray diffraction pattern collected for the synthesized iron sulfide nanomaterial.

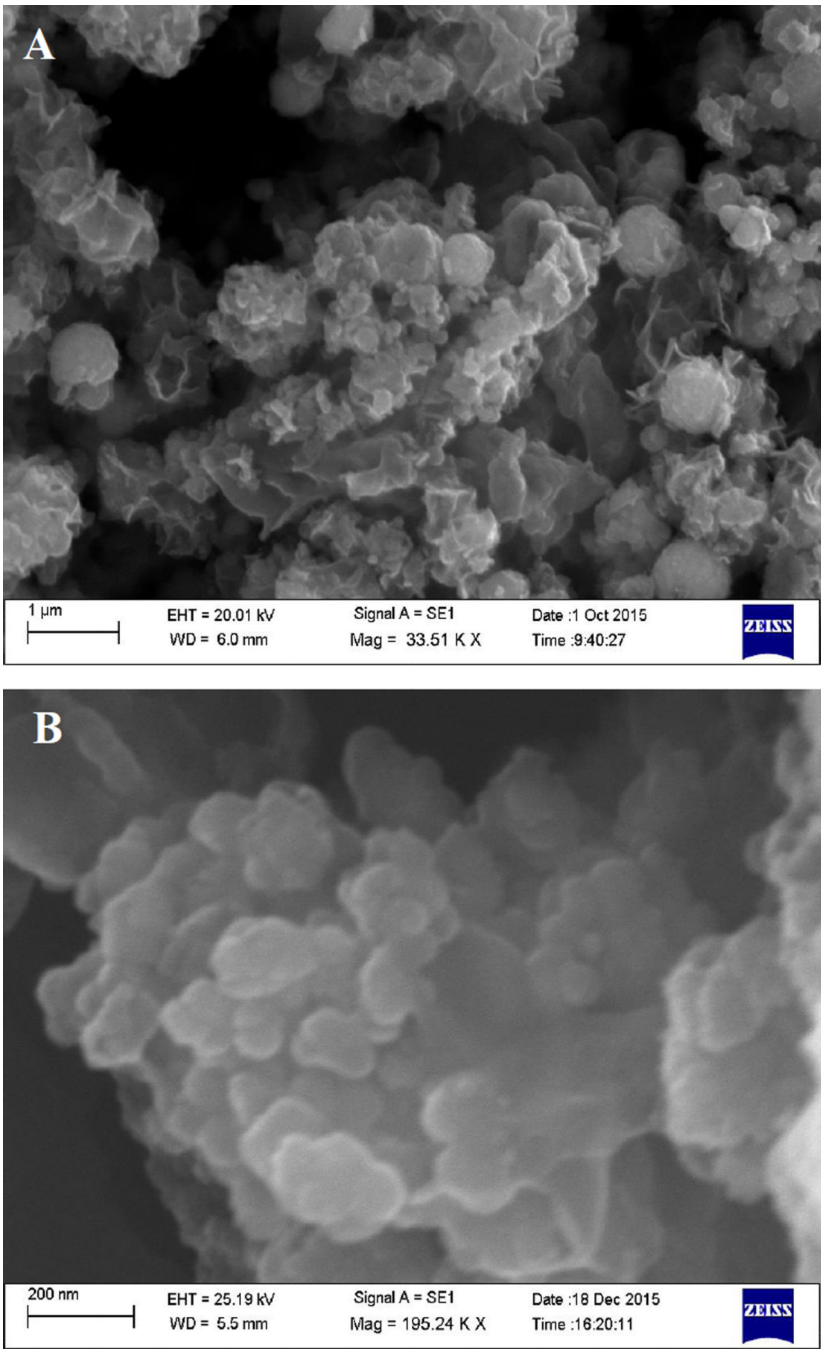

Figure 2.
SEM images of the synthesized Fe7S8 nanomaterial.

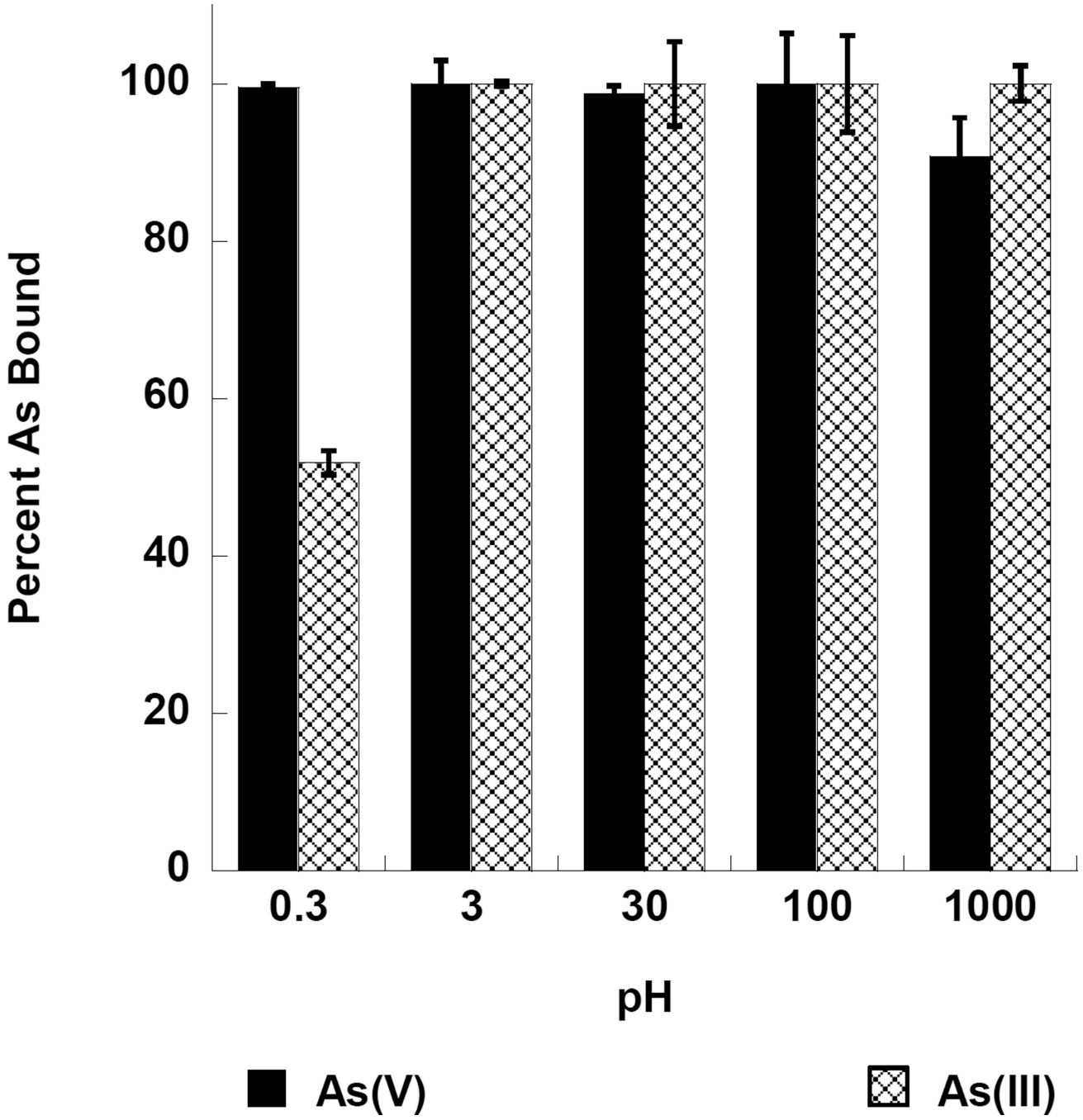

Figure 3.
pH dependence of the adsorption of As(III) and As(V) binding to the Fe_7S_8 nanomaterial.

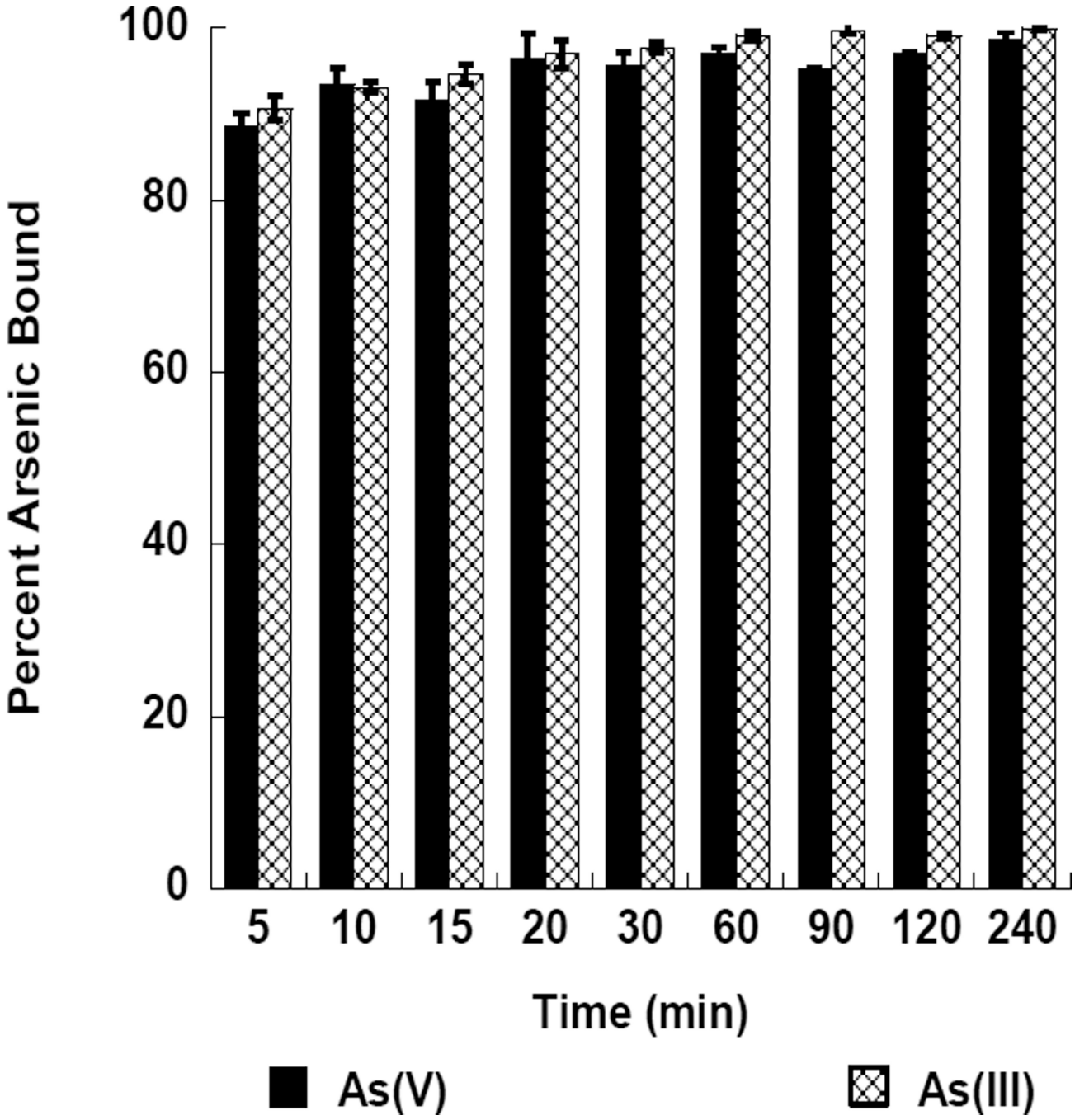

Figure 4.
Time dependency for the adsorption of As(III) and As(V) binding to the Fe_7S_8 nanomaterial.

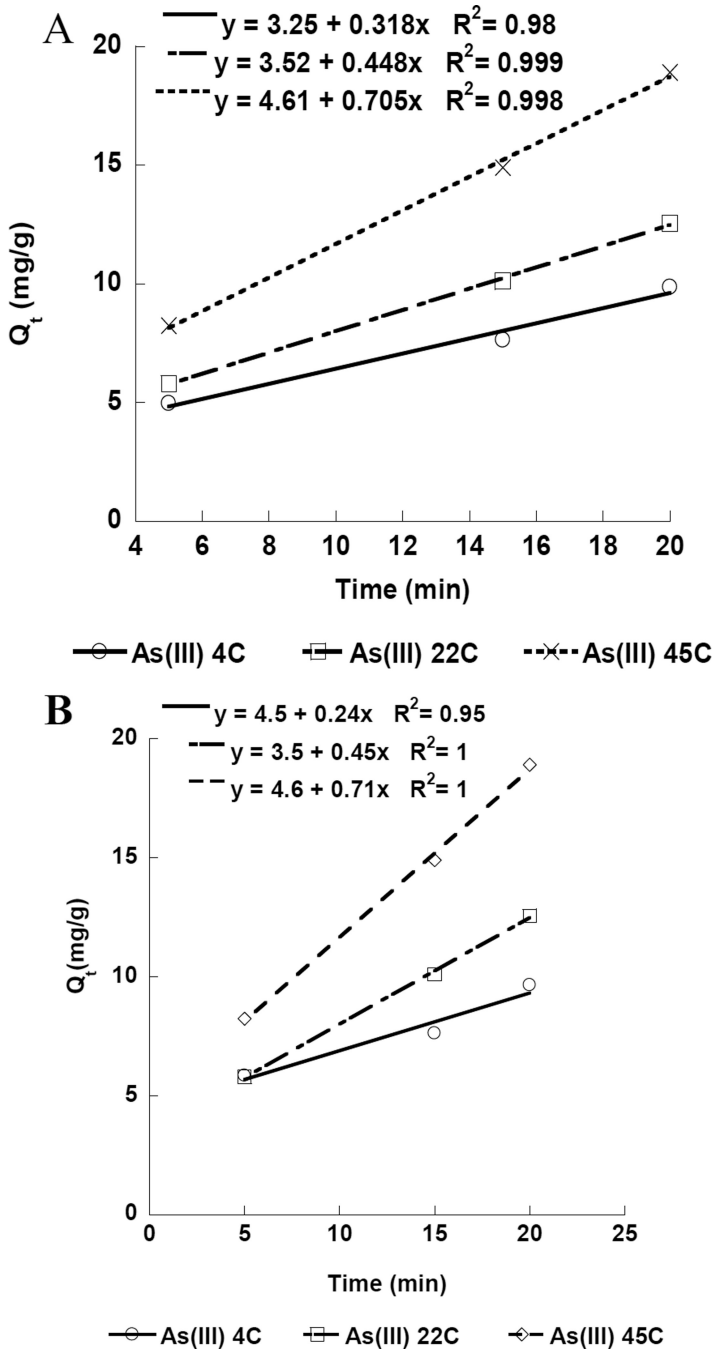

Figure 5.

Kinetics plot for the adsorption of As(III) (A) and As(V) (B) binding to the Fe_7S_8 nanomaterial at 45°C, 22°C, and 4°C.

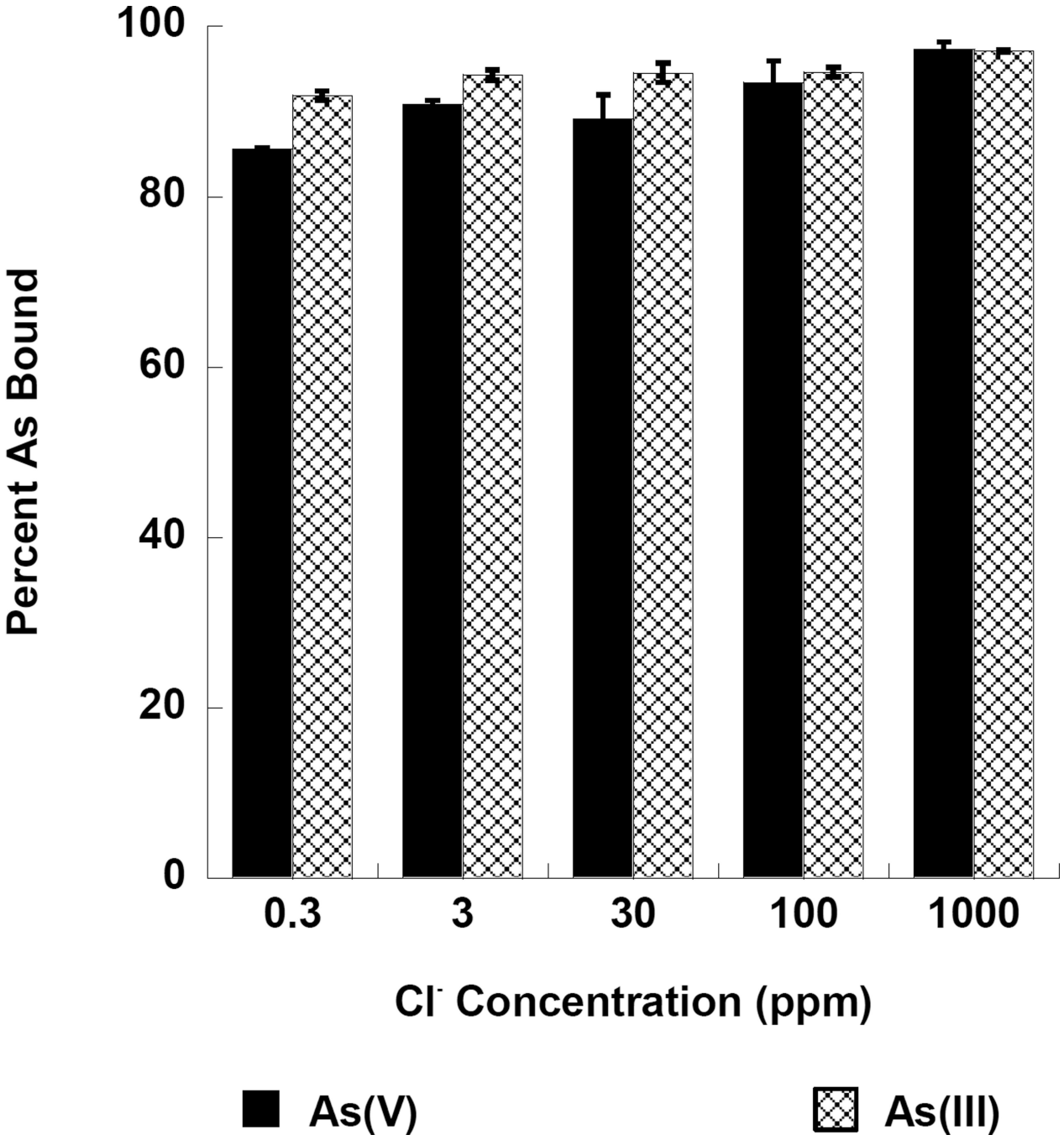

Figure 6.
Effect of Cl^- interference adsorption of As(III) and As(V) binding to the Fe_7S_8 nanomaterial.

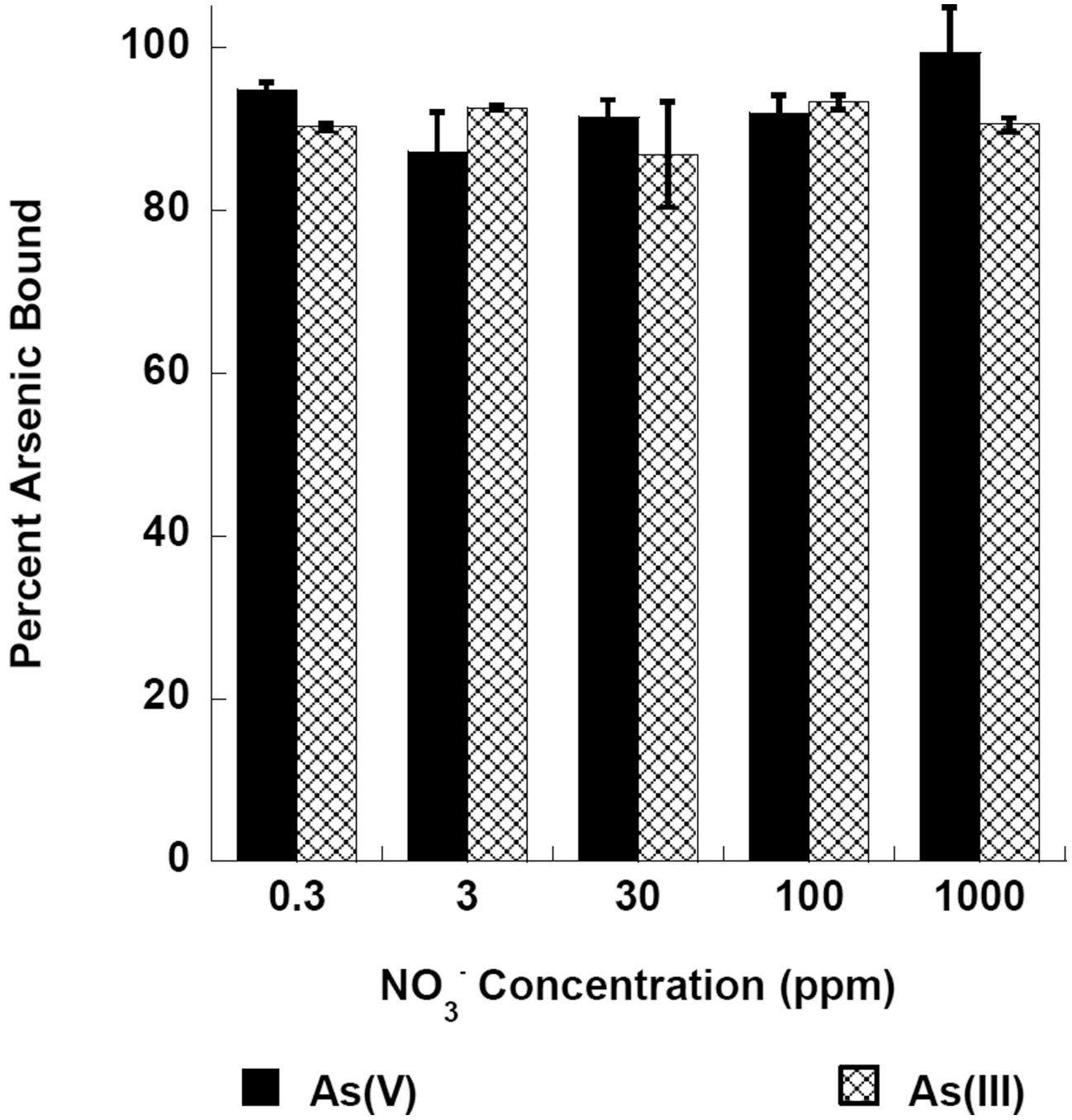

Figure 7.
Effect of NO^{3-} interference adsorption of As(III) and As(V) binding to the Fe_7S_8 nanomaterial.

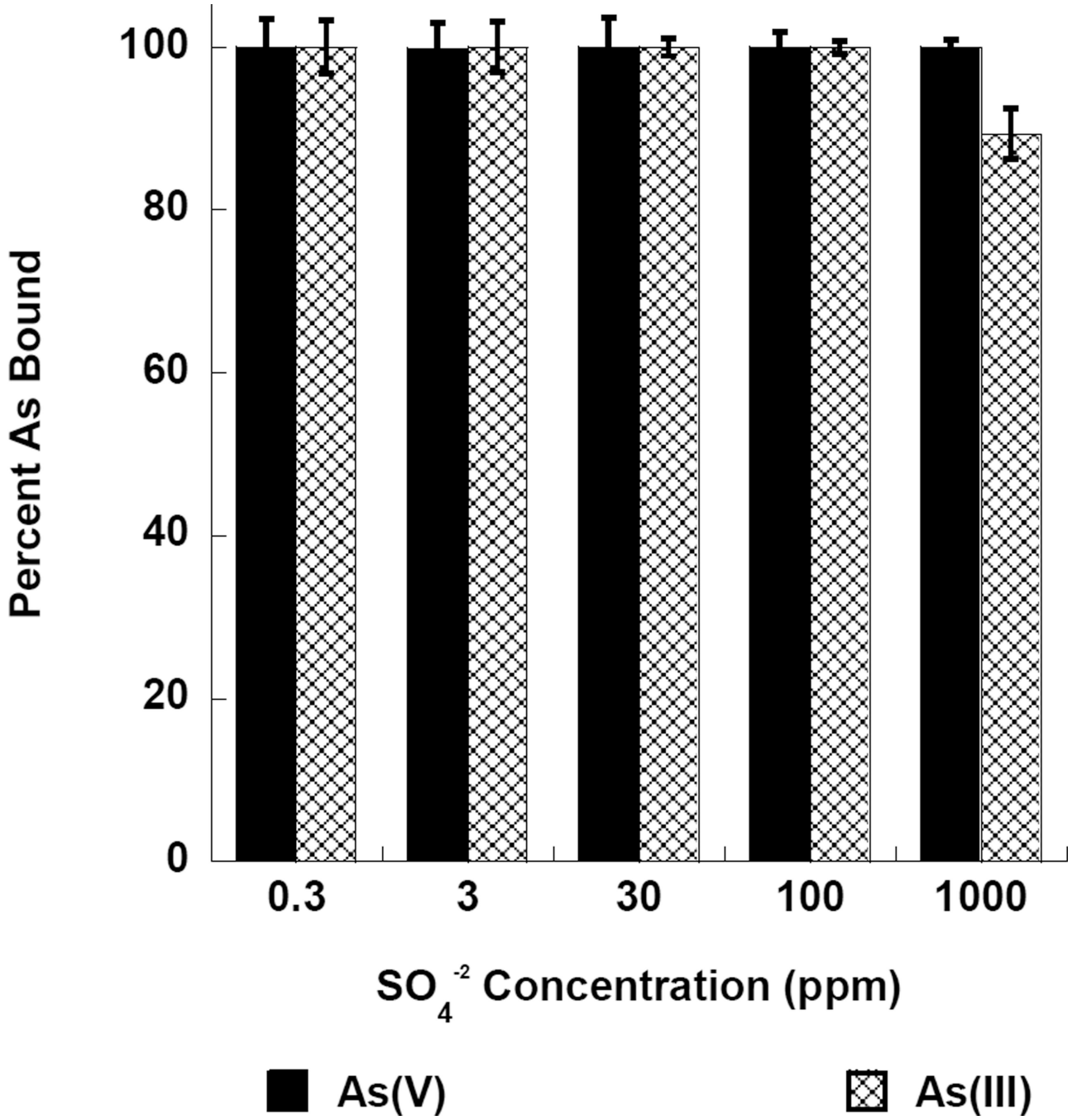

Figure 8.
Effect of SO_4^{2-} interference adsorption of As(III) and As(V) binding to the Fe_7S_8 nanomaterial.

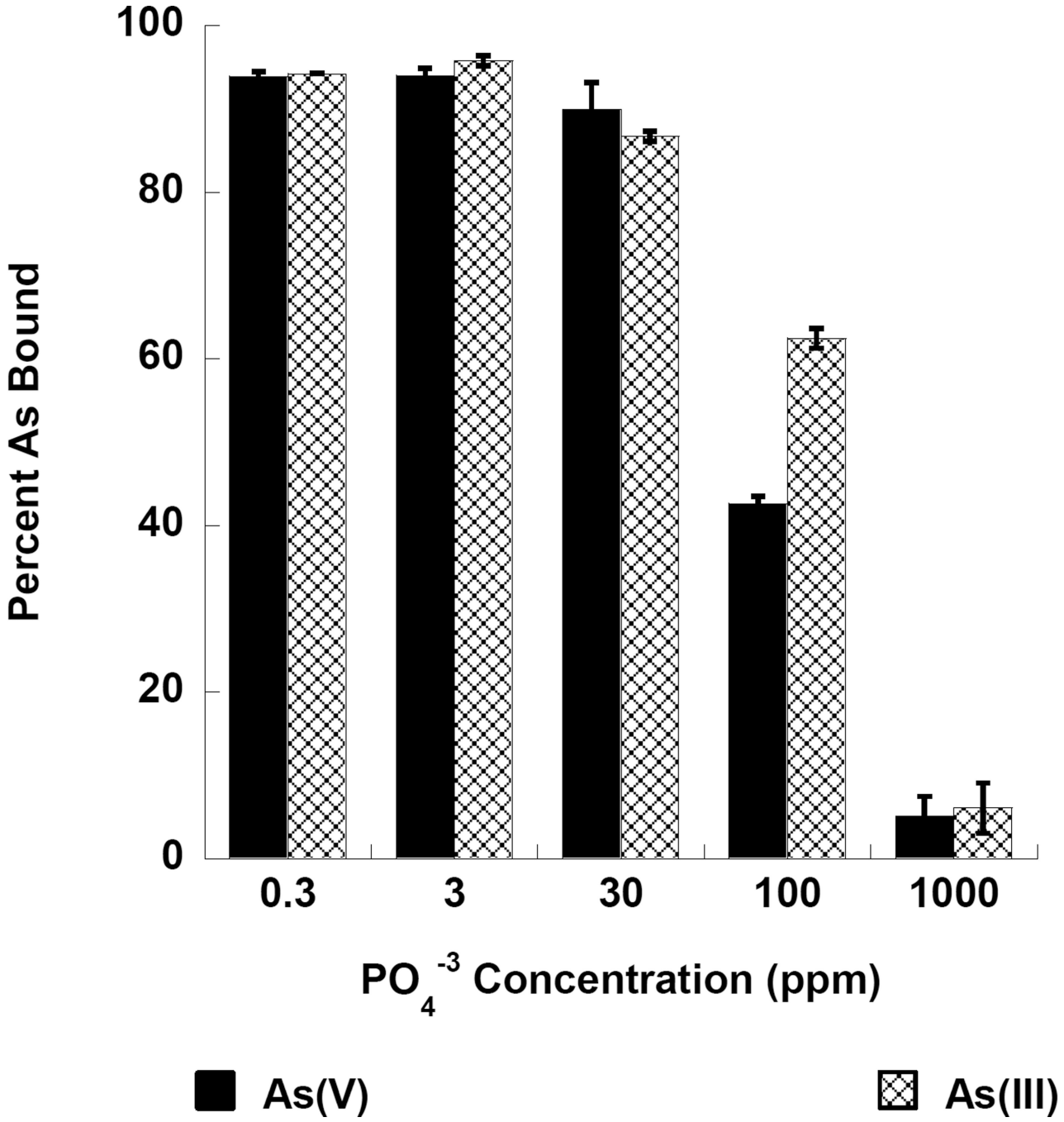

Figure 9.
Effect of PO_4^{3-} interference adsorption of As(III) and As(V) binding to the Fe_7S_8 nanomaterial.

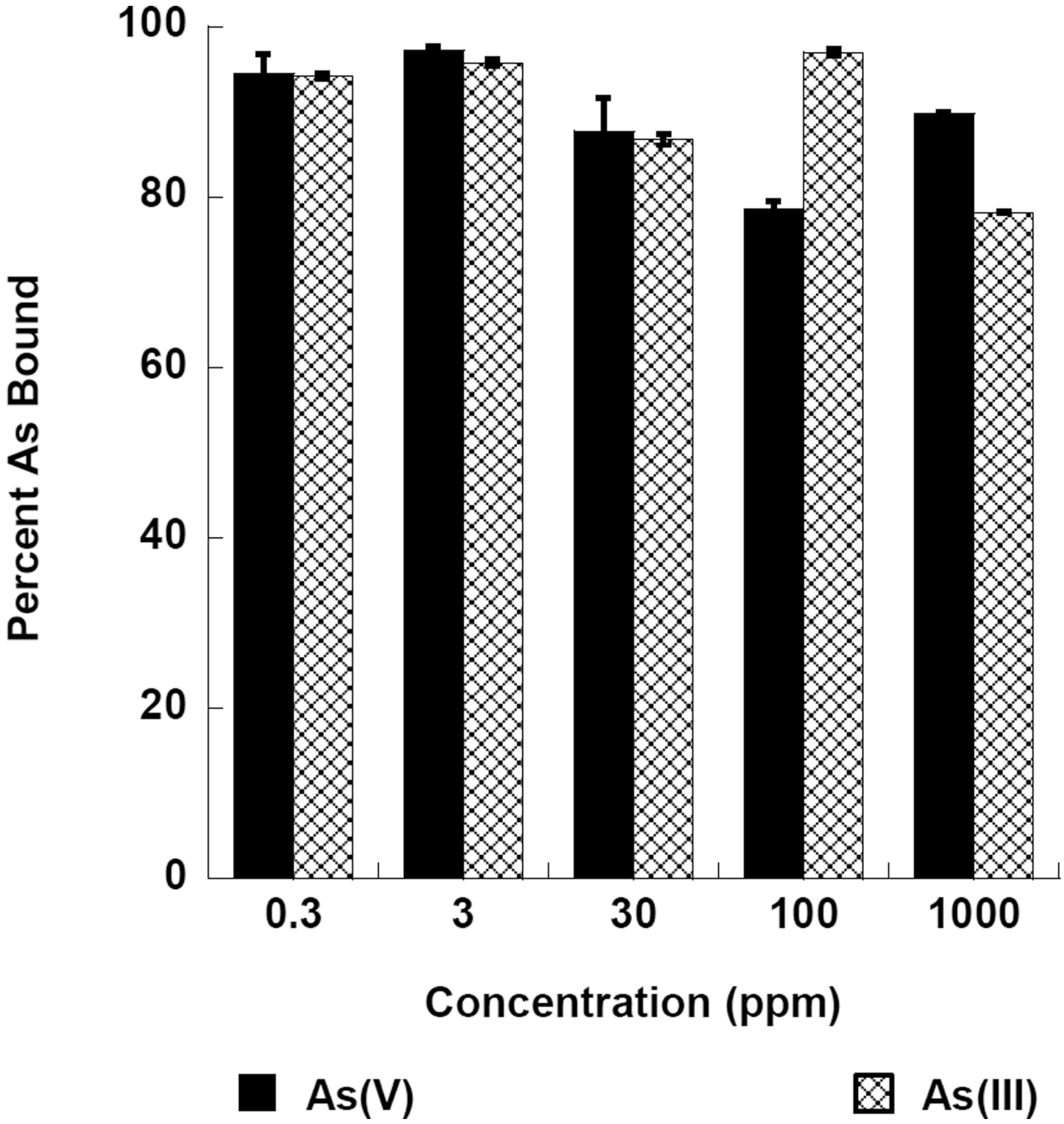

Figure 10.

Effect of combined interferences Cl^{-}, NO_3^{-}, SO_4^{2-}, and PO_4^{3-} adsorption of As(III) and As(V) binding to the Fe_7S_8 nanomaterial at 45°C, 22°C, and 4°C.

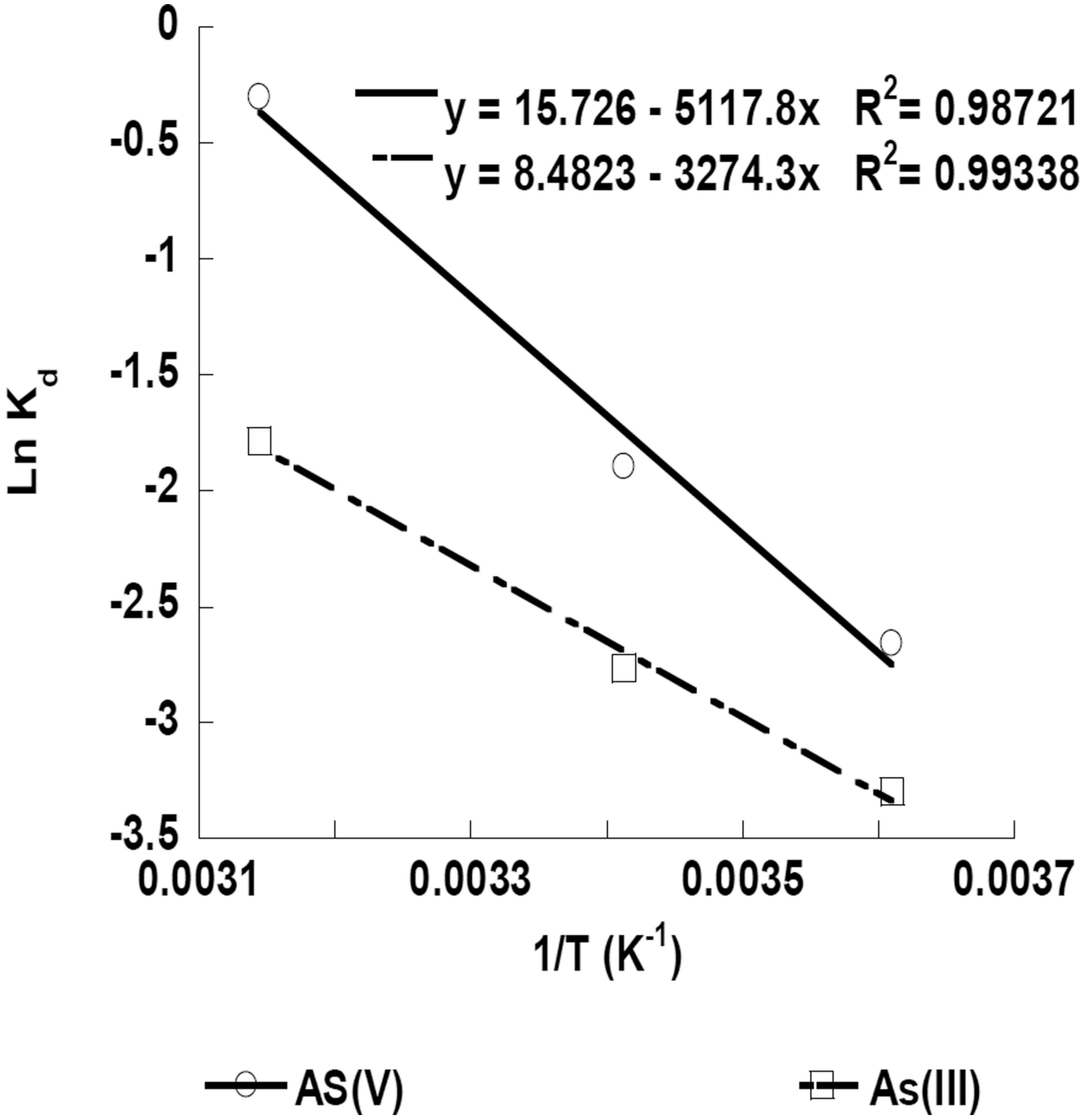

Figure 11.
Thermodynamics plot of the binding of As(III) and As(V) binding to the Fe_7S_8 nanomaterial at 45°C, 22°C, and 4°C.

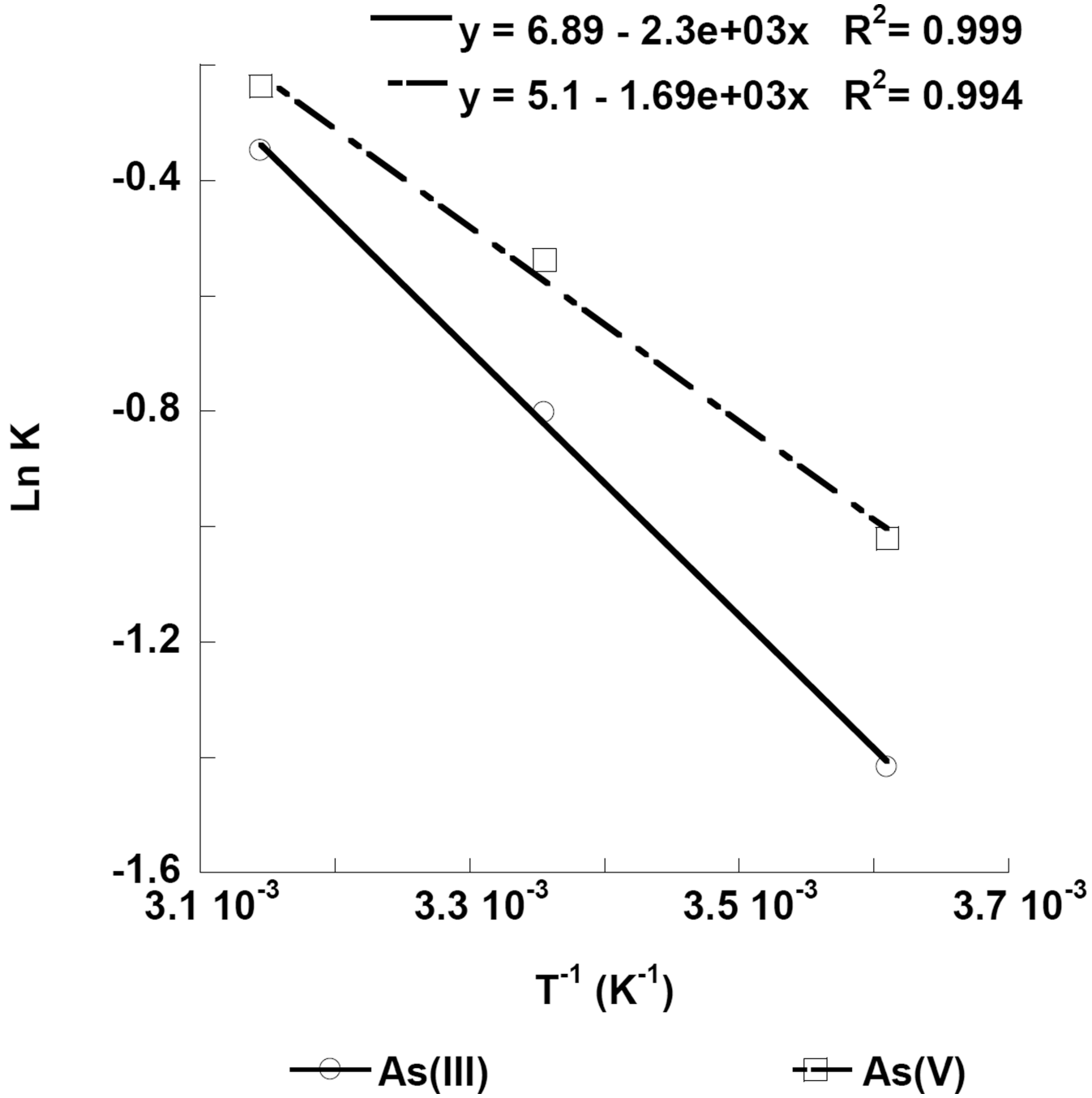

Figure 12.
Arrhenius plot for the adsorption of As(III) and As(V) binding to the Fe_7S_8 nanomaterial.

Table 1

GFAAS parameters used for the analysis of As(III) and As(V) concentrations in solution after reaction with the nanoadsorbent at a λ 19.37 nm.

	Temperature (°C)	Ramp time (s)	Hold time (s)
Pre-dry	110	1	30
Dry	130	15	30
Char	1200	10	20
Atomization	2000	0	5
Clean out	2400	1	2

Table 2

ICP-OES parameters used for the analysis of As(III) and As(V) concentrations in solution after reaction with Fe_7S_8 nanomaterial.

Parameter	Setting
λ	193.7 nm
RF power	1500 W
Nebulizer	Gemcone (low flow)
Plasma Flow	15 L/min
Auxiliary Flow	0.2 L/min
Nebulizer Flow	0.55 L/min
Sample Flow	1.50 mL/min
Injector	2.0 mm Alumina
Spray Chamber	Cyclonic
Integration Time	20 seconds
Replicates	3

Table 3

Binding capacity of the Fe_7S_8 nanomaterial for arsenic(III) and arsenic(V) using the Langmuir isotherm.

Arsenic Form	Equation	R^2	Capacity (mg/g)
As(III)	Y=0.3267X+.0698	0.99	14.3
As(V)	Y= 0.078X+.0319	1.0	31.3

Table 4

Calculated Thermodynamic Parameters for the adsorption of arsenic(III) and arsenic(V) to the Fe_7S_8 nanomaterial.

Arsenic Form	Ea (kJ/mol)	ΔG (kJ/mol)	ΔH (kJ/mol)	ΔS (J/mol)
As(III)	19.1	7.59(277K)	27.2	70.50
		6.73 (295 K)		
		4.71(318K)		
As(V)	14.1	6.12(277K)	42.5	131.03
		4.62 (295 K)		
		0.80 (318K)		